ROYAL SOCIETY
OF CHEMISTRY

PAPER

Check for updates

Stain-resistant, superomniphobic flexible optical plastics based on nano-enoki mushroom-like structures†

Sajad Haghanifar, [ID] [a] Luke M. Tomasovic, [ID] [b] Anthony J. Galante, [ID] [a] David Pekker[c] and Paul W. Leu [ID] *[ad]

In this paper, we demonstrate the stain-resistance and high pressure stability of superomniphobic flexible optical plastics. A scalable method for creating nano-enoki mushroom-like structures in plastics is presented that provides the re-entrant geometry needed to prevent infiltration from a variety of liquids. The surface demonstrates static contact angles over 150° and low contact angle hysteresis under 20° for a wide variety of organic liquids. The re-entrant tops and fluorination of the nano-enoki as well as the few micron spacing between nanostructures provide robust metastable solid–liquid–air interfaces in the presence of Laplace pressures of at least 900 Pa. In addition, compared to the initial bare plastic, the nano-enoki structures demonstrate comparable transmission values (86.4% *versus* 88.4% at a wavelength of 550 nm) and ultrahigh haze values (96.4% *versus* 1.1%). The surfaces exhibit stain-resistance for a variety of liquids including mustard and blood, where mustard and dried blood both flake off the samples without any residue. We also performed durability experiments which demonstrate that nano-enoki plastics are robust to bending with similar transmission, haze, wetting contact angle, and hysteresis values after 5000 cycles of bending.

Introduction

There has been tremendous research interest in super-hydrophobic surfaces, which strongly repel water, and can provide functionalities such as anti-fogging,[1] anti-icing,[2] and self-cleaning.[3,4] In addition, there is great interest in extending this repellency beyond water. Surfaces that repel oils may be referred to as oleophobic, and surfaces that repel a wide range of liquids may be referred to as omniphobic. A variety of re-entrant geometry structures have been demonstrated that can effectively impede penetration by various liquids, such as T-shaped microstructures,[5] mushroom-like micropillars,[6–8] porous membranes,[9] and springtail-inspired surfaces.[10] Super-omniphobicity may be used for self-cleaning surfaces,[11] chemical shielding surfaces,[12] and stain-free clothing.[13,14]

There is also great interest in combining these functionalities with photon management properties, such as high transparency and haze control which are of importance for optoelectronic applications as well as providing these functionalities to flexible materials which are needed for flexible versions of existing optoelectronic applications as well as emerging wearables, RF-ID tags, artificial skin, and medical sensors.[15,16] High transparency and low haze surfaces[17–19] are desirable for applications such as displays, as low haze provides clarity of text and images. In contrast, omniphobic substrates with high transparency and high haze are desirable for opto-electronic applications such as light emitting diodes and solar cells. Substrates with high haze can increase the amount of light scattered into or out of photoactive layers and may increase the power conversion efficiency and extraction efficiency of solar cells[20] and LEDs,[21] respectively. Substrates with both high transparency and high haze are difficult to obtain as surfaces with high transmission tend to have low haze.[22,23]

So far, the only work on omniphobic substrates with high transparency and high haze has been the work of Jeong *et al.*, where they reported a PET substrate with a silica nanoparticle coating that improves the photon-to-electron conversion efficiency of organic solar cells by 13% compared to that on a PET substrate without the silica nanoparticle array layer.[24] However, the transparency of these coated substrates is fairly low at less than 80%. Furthermore, the sample demonstrates a contact angle of 139° for ethylene glycol, which still has a relatively high surface tension of 47.7 mN m^{-1}. The demonstration of super-omniphobicity with low liquid surface tension liquids such as

[a]Department of Industrial Engineering, University of Pittsburgh, Pittsburgh, PA 15261, USA. E-mail: pleu@pitt.edu
[b]Department of Chemical and Biomolecular Engineering, Georgia Institute of Technology, Atlanta, GA 30332, USA
[c]Department of Physics, University of Pittsburgh, Pittsburgh, PA 15261, USA
[d]Department of Mechanical Engineering, University of Pittsburgh, Pittsburgh, PA 15261, USA
† Electronic supplementary information (ESI) available. See DOI: 10.1039/c9ta01753d

hexadecane, which has a surface tension of 27.7 mN m^{-1}, while offering high transparency and high haze performance, has yet to be demonstrated.

In this paper, we demonstrate stain-resistant super-omniphobic flexible optical plastics with nano-enoki mushroom-like structures that may be fabricated through scalable processes. Our nano-enoki polyethylene terephthalate (PET) has re-entrant geometry and close spacing between structures to provide both high apparent contact angles > 150° and low contact angle hysteresis for a wide variety of liquids of varying surface tension such as water, ethylene glycol, olive oil, and hexadecane. The nano-enoki structures exhibit high pressure stability due to the few micron-scale spacing between our nanostructures, which provides a large energy barrier to water infiltration. The spacing between our nanostructures is the closest in the literature that we are aware of for re-entrant superomniphobic structures. Our nano-enoki structures exhibit no evidence of water breakthrough at pressures over 900 Pa, which demonstrates the high meta-stability of Cassie–Baxter state wetting. Furthermore, the nano-enoki PET exhibits a high transmission and ultrahigh haze of 86.4% and 96.4%, respectively, at a wavelength of 550 nm, which may be suitable for some optical applications.

The surfaces exhibit stain-resistance for a variety of liquids including mustard and blood, where the transparency of the original plastic is recovered after staining. Dried mustard and blood both flake off the samples without any residue, indicating no infiltration of the liquid and poor adhesion to the surface. We also performed durability experiments that demonstrate that these nanostructured PET substrates are robust to bending and show similar transmission, haze, contact angle and hysteresis values after 5000 cycles of bending.

Experimental

Nano-enoki plastic fabrication process

The nano-enoki PET structures are created through a maskless reactive ion etching (RIE) fabrication process,[25] followed by plasma enhanced chemical vapor deposition (PECVD) silica deposition, and fluorination. The 125 μm thick PET substrate is etched with CF_4 and O_2 with flow rates of 45 and 5 sccm, respectively. The total pressure of the chamber is maintained at 150 mTorr and the power is set at 125 W. Polymer particles are deposited on the PET surface during this etching process, acting as a nano-mask for creating high aspect ratio structures.[26] The height of the nanostructures may be controlled by the etching time and the etching rate was approximately 300 nm min^{-1}. Next, SiO_2 is deposited on top of the high aspect ratio nanostructures by PECVD at 200 °C to avoid melting of the PET substrate. The pressure of the chamber and the power are set at 900 mTorr and 60 watt, respectively. The flow rates of SiH_4/N_2 and N_2O were both 140 sccm. The thickness of the SiO_2 layer can be controlled by the deposition time, which was approximately 100 nm min^{-1}. Trimethoxy(1H,1H,2H,2H-hep-tadecafluorodecyl)silane (Sigma-Aldrich) with a volume of 0.05 mL was vapor-deposited on the nano-enoki PET in a vacuum chamber at 30 mTorr. A vapor deposition time of 16 h was used which provided a uniform coating.

Wetting characterization

Four different types of liquid droplets of 5 μL volume with various surface tensions were deposited on the PET substrates and the lotus leaf for comparison. Deionized water, Sigma-Aldrich hexadecane, Sigma-Aldrich ethylene glycol, and grocery store extra virgin olive oil were used. An Attension Theta optical tensiometer was used to measure the contact angle and hysteresis of different samples. Three measurements were made for each sample and the mean and standard deviation for each one are reported. The advancing and receding contact angels were obtained by the sessile drop method where water is slowly pumped into or out of the droplet. The hysteresis value is the difference between advancing and receding contact angles.

Optical characterization

A spectrophotometer (PerkinElmer, Lambda 1050) equipped with a 150 mm integrating sphere was used for measuring the total transmission of the sample between 400 and 1200 nm wavelengths. The integrating sphere was removed for measuring the direct transmission of the samples. The scattering angular distribution was measured using a Cary 7000 Universal Measurement Spectrophotometer (UMS). In this instrument, incident light is normal to the sample surface with a 5 mm × 5 mm square beam and the photodetector is scanned from 10 to 350 (−10) degree. The wavelengths are measured from 530 to 570 nm.

Stain test

5 mL of Heinz yellow mustard and heparinized porcine blood collected in necropsy of swine were placed on the samples, and evaporated at room temperature for 24 hours. The samples were then tilted at 90°. Optical measurements were performed both before and after stain tests.

Results and discussion

Fig. 1 shows details and results of the nano-enoki mushroom structures on PET and compares them to those of the *Nelumbo nucifera* or sacred lotus leaf surface. Fig. 1a shows results of the enoki mushroom-like nanostructures. Fig. 1a(i) shows 20° tilted cross-section scanning electron microscopy (SEM) images and Fig. 1a(ii) shows an overhead SEM image. The nanostructures shown here are initially 18 μm in height after etching for 60 minutes. The structures have a diameter of about 50–100 nm at the bottom which gradually increases to 200–500 nm at the top. The overhead SEM image shows some coalescence of nano-structures during the SiO_2 deposition. Fig. 1a(iii) shows a picture of actual enoki for comparison, where the mushrooms have larger tops and a long string-like appearance.

The structures are formed by first etching the PET with a maskless RIE process,[25,27] then coating the nanostructures with a silica layer by PECVD and finally, treating the structures with a low surface energy fluorosilane. Fig. 1b(i) and (ii) show the SEM images of the surface without and with fluorinated tops. The nano-enoki structures without fluorinated tops are the structures just after the RIE process, without the additional
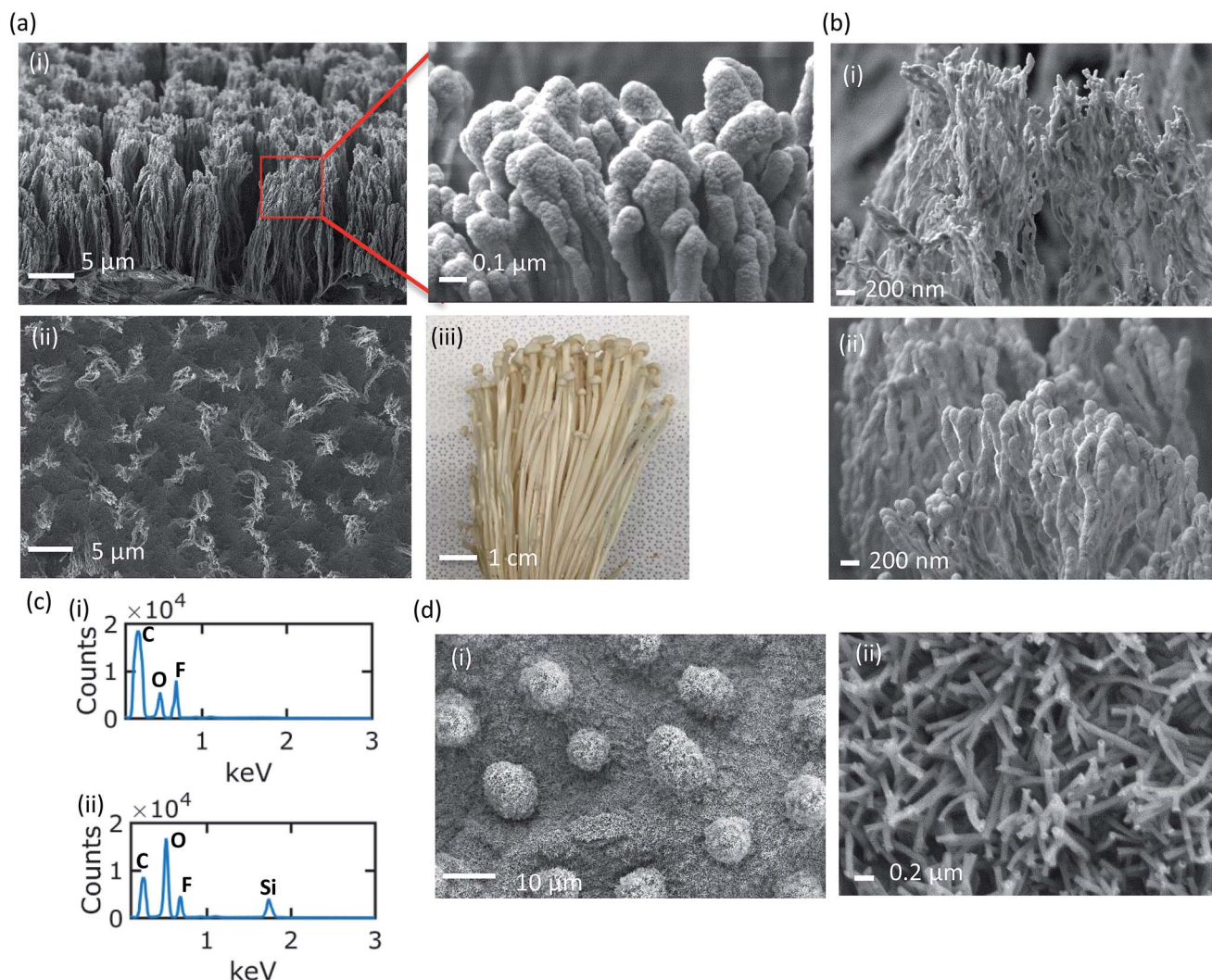
Fig. 1 (a) Nano-enoki mushroom structures on PET. (i) 20° tilted cross-section scanning electron microscopy (SEM) images and (ii) overhead SEM images. (iii) Optical image of enoki mushrooms. (b) Side view SEM images of nano-enoki PET (i) without and (ii) with fluorinated tops. (c) Energy dispersive X-ray spectroscopy (EDS) data of the samples (i) without and (ii) with fluorinated tops. (d) SEM images of the lotus leaf surface at different resolutions demonstrating (i) microstructure bumps and (ii) nanostructures.

PECVD and fluorination. The PECVD process tends to deposit silica on top of the nanostructures instead of the bottom, thus creating re-entrant enoki mushroom-like nanostructures. Fig. 1c shows the energy dispersive X-ray spectroscopy (EDS) data of the samples (i) without and (ii) with fluorinated tops. The fluorine in the composition comes from the CF_4 gas used for etching. Since the formation of fluorinated tops includes the deposition of silica, the peak associated with silicon appears in EDS data after fluorination. The subsequent fluorosilane treatment forms a monolayer of fluorosilane on the structure.[28] For comparison purposes, we provide SEM images of the lotus leaf in Fig. 1d. The lotus leaf surface consists of micron-sized papillae (Fig. 1d(i)) with nanometer-size protrusions (Fig. 1b(ii)) and a surface layer of epicuticular wax. Superhydrophobic surfaces are inspired by the leaves of the sacred lotus plant, which are both anti-fouling and self-cleaning due to the combination of hierarchical surface morphology and hydrophobic epicuticular wax.[29]

Wetting characterization of the nano-enoki PET and lotus leaf was performed with water (surface tension of 72.8 mN m^{-1}), ethylene glycol (47.7 mN m^{-1}), olive oil (32.0 mN m^{-1}), and hexadecane (27.5 mN m^{-1}). Fig. 2a shows the static contact angles of these four liquids for the 18 μm tall nano-enoki PET as compared to the lotus leaf. The lotus leaf is superhydrophobic with a static contact angle of 160 ± 2° for water. However, lower surface tension liquids tend to spread more easily and have lower static contact angles. The contact angles are 40 ± 3° and 7 ± 2° for olive oil and hexadecane, respectively, which tend to spontaneously spread on the lotus leaf surface. Not only does the nano-enoki PET exhibit high static water contact angles, but also high contact angles for the other liquids tested above 150°. The nano-enoki PET exhibits contact angle values of 172 ± 1.5°, 161 ± 1.6°, 156 ± 1.5° and 153 ± 1.7°, for water, ethylene glycol, olive oil and hexadecane, respectively.

Fig. 2b plots the contact angle hysteresis for the four liquids for both the lotus leaf and the nano-enoki. The large hysteresis
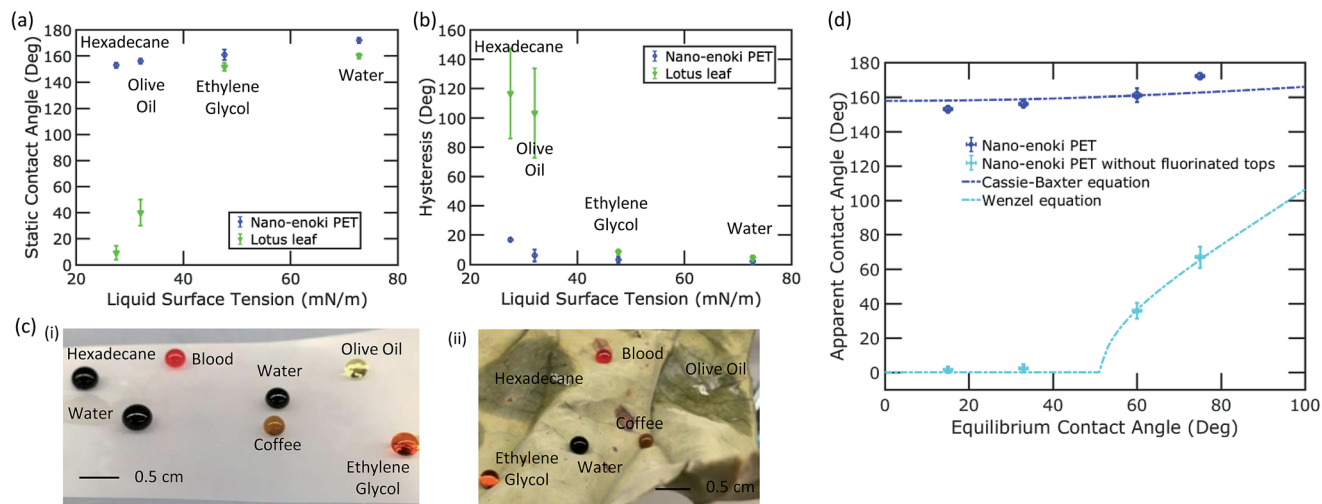
Fig. 2 Surface wetting results. (a) The apparent contact angle variation of 18 µm tall nano-enoki PET and lotus leaf for water, ethylene glycol, olive oil, and hexadecane. (b) Hysteresis of different liquids with different surface tensions on the 18 µm tall nano-enoki PET and lotus leaf. (c) Optical picture of various liquids on the (i) plastic demonstrating superomniphobicity and (ii) the lotus leaf demonstrating superhydrophobicity, but inability to repel the lower surface tension liquids of olive oil and hexadecane. (d) Plot of apparent contact angles *versus* equilibrium contact angles of four different liquids for nano-enoki and nano-enoki without fluorinated tops. The Cassie−Baxter equation and Wenzel equation are also plotted with estimates of the solid−liquid area fraction and roughness. The dotted lines come from standard error estimates.

values of the olive oil and hexadecane on the lotus leaf are indicative of strong adhesion to the surface. For the nano-enoki PET, the contact angle hysteresis for the four liquids is $2.0 \pm 0.6°$, $3.0 \pm 0.5°$, $6.0 \pm 2.0°$ and $17.0 \pm 1.2°$, respectively. The high apparent contact angles and small hysteresis angles of the re-entrant nano-enoki mushrooms for a wide range of liquids demonstrate the superomniphobicity of these structures. The droplets easily roll off the surface due to the repellency of the liquids. Fig. 2c(i) shows an optical image of different liquids on the 18 µm superomniphobic enoki mushroom-like nano-structured PET. The superomniphobic surface demonstrates repellency for a wide variety of liquids beyond those evaluated, including blood and coffee. Fig. 2c(ii) shows an optical image of different liquids on a lotus leaf. The lotus leaf shows high apparent contact angles for water, ethylene glycol, blood and coffee. However, the olive oil and hexadecane droplets spread spontaneously on the leaf.

The fluorination of the surface was measured by comparison of different water and oil contact angles of the surface with and without fluorinated tops. To examine the importance of re-entrant structures and fluorination in promoting Cassie–Baxter state wetting, we compared the wetting properties of our 18 µm tall nano-enoki PET to the same structures without fluorinated tops. Fig. 2d plots the experimentally measured apparent contact angles of the nano-enoki PET as well as the nano-enoki PET without the fluorinated tops for water, ethylene glycol, olive oil and hexadecane. The apparent contact angles of the four liquids on the nano-enoki PET were compared with that predicted from the Cassie–Baxter equation:

$$\cos(\theta^*) = f_{SL} \cos(\theta_E) - f_{LV} \tag{1}$$

where f_{SL} is the areal fraction of the solid–liquid interface, f_{LV} is the areal fraction of the liquid–vapor interface, θ^* is the

apparent contact angle, and θ_E is the equilibrium contact angle. $f_{SL} + f_{LV} = 1$. f_{SL} was treated as a fitting parameter, and the curve fit shown is with $f_{SL} = 0.04$, which is consistent with estimates from overhead SEM pictures. The θ_E values are the contact angles of different liquids on plain PET. θ_E was measured to be $75.0 \pm 1.0°$, $60.0 \pm 1.0°$, $33.0 \pm 1.0°$ and $15.0 \pm 1.0°$ for water, ethylene glycol, olive oil and hexadecane, respectively. The prediction from the equation agrees well with the measured apparent contact angles indicating that the liquids are indeed in the Cassie–Baxter state of wetting.

We further compare the experimentally measured apparent contact angles for the nano-enoki PET without fluorinated tops with the predicted apparent contact angles from the Wenzel equation:

$$\cos(\theta^*) = r \cos(\theta_E) \tag{2}$$

where the value of surface roughness r is estimated as $r = 1.5$ for the 18 µm tall nano-enoki PET without fluorinated tops with a diameter of 225 nm and pitch of 5 µm. As can be seen from the plot, our experimental data agree well with that predicted from the Wenzel equation. For liquids with an equilibrium contact angle less than 50°, such as hexadecane and olive oil, the liquid completely spreads over the nanostructured surface. In the cases where the surface has an affinity for the liquid (equilibrium contact angle less than 90°), the Wenzel wetting state is enhanced by nanostructuring and decreases the wetting contact angle.[30] The fluorinated tops of the nano-enoki are critical for creating low surface energy re-entrant structures that promote Cassie–Baxter state wetting as opposed to the Wenzel state. The low contact angle fraction between the droplets and plastic in the Cassie–Baxter wetting state enables high apparent contact angles and low contact angle hysteresis.

Fig. 3 shows the wetting results of different nano-enoki substrates of varying heights. Different height nano-enoki substrates were fabricated by varying the RIE etching time, while the PECVD and fluorination process were kept the same. Fig. 3 shows the (a) apparent contact angle and (b) contact angle hysteresis for different liquids with different surface tensions on various height nano-enoki substrates. In all cases, the nano-enoki substrates perform better than the lotus leaf. The water and ethylene glycol contact angles for all the nano-enoki samples are more than 150°, and the water hystereses are less than 10°. However, static contact angles greater than 150° and water hysteresis less than 20° are true for hexadecane and olive oil only for the nano-enoki substrates that are 18 μm or taller.

To further understand the wetting behavior on nano-enoki nanostructures of different heights, we characterized the stability of the metastable Cassie–Baxter wetting state of droplets on our nano-enoki nanostructures. A 5 μL drop of water was placed on each substrate and evaporated while monitoring the decrease of the contact angle. Fig. 3c plots the evolution of the contact angle as a function of time and Fig. 3d plots the contact angle as a function of the baseline diameter. In all surfaces, the contact angle decreased continuously without any evidence of pinning due to the low contact angle hysteresis of the surfaces and without any sudden discontinuities in the contact angle.

The decreasing contact angle is indicative of gradual infiltration of water into the structures. However, only the 4 μm tall nano-enoki exhibited a decrease in the contact angle without a concomitant decrease in the baseline diameter, indicative of breakthrough into the Wenzel wetting state. In these shorter nano-enoki structures, the droplet may transition into the Wenzel state at lower pressures as it is easier for the droplet to droop and touch the bottom of the space between nano-enoki structures as the pressure increases.[31]

The breakthrough pressure is the maximum external pressure that the surface can tolerate before transition from the Cassie–Baxter state to the Wenzel state.[32] The robustness factor A^* is a measure of the metastability of the Cassie–Baxter state for a given surface:[32–34]

$$A^* = P_{breakthrough}/P_{ref} \qquad (3)$$

where $P_{breakthrough}$ is the breakthrough pressure at which the surface wetting transitions to the Wenzel state, and P_{ref} is a reference pressure given by

$$P_{ref} = 2\gamma_{LV}\Big/\sqrt{\gamma_{LV}/\rho g} \qquad (4)$$

where ρ is the liquid density, and g is the gravitational acceleration.[32] When A^* is less than 1, the composite solid–liquid–air
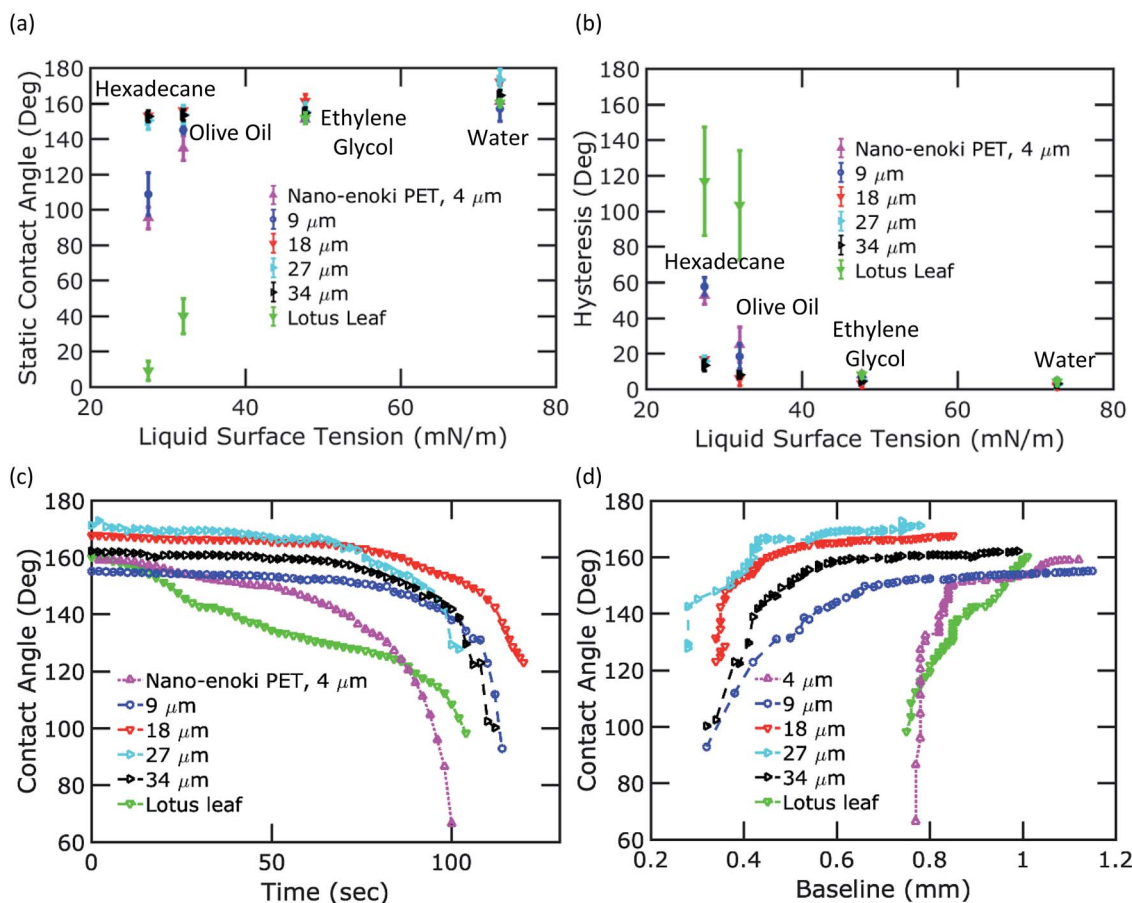

Fig. 3 (a) Static contact angle and (b) hysteresis of different liquids on samples with different height nano-enoki surfaces. Contact angle as a function of (c) time and (d) baseline for nano-enoki of different heights and lotus leaf.

interface cannot be supported and the Cassie–Baxter state is not metastable.

A minimum 160 μm droplet radius was observed in the nano-enoki PET without any breakthrough. This corresponds to a breakthrough pressure over 900 Pa and robustness factor more than 17. Other studies in the literature such as mushroom-shaped micropillar arrays[7] or hierarchical structures[33] exhibit lower breakthrough pressures or lower robustness factors as those structures are over 20 microns apart from each other. In contrast, the spacing of our nano-enoki structures is only approximately 5 μm and thus provides a much larger energy barrier for water infiltration that increases the robustness of the Cassie–Baxter wetting state and super-hydrophobicity. The spacing of the nano-enoki structures is the smallest in the literature that we are aware of for super-omniphobic re-entrant structures. Back-of-the-envelope calculations with a spacing of 5 μm, and 9 μm height and a diameter of 300 nm suggest that the water droplet will only come into contact with the bottom of the cavity when the radius of the droplet is smaller than the spacing or 5 μm.[31] A droplet of radius 5 μm would have a breakthrough pressure of 28 kPa.

The nano-enoki structures exhibit high transparency and high haze, which make them suitable as an optical plastic. Compared to the initial bare plastic, the nano-enoki structures demonstrate comparable transmission values (86.4% *versus* 88.4% at a wavelength of 550 nm) and ultrahigh haze values (96.4% *versus* 1.1%). The transparency and haze are similarly high between 400 and 1200 nm wavelengths. The sub-wavelength nature of the nano-enoki provides high scattering and high transparency which is not possible with larger structures.

Fig. 4 summarizes the optical results of the samples. Fig. 4a shows the total transmission of the nano-enoki as a function of height from 400 to 1200 nm. The transmission at a height of 0 μm corresponds to flat PET. Initial creation of the nano-enoki PET corresponds to a reduction in transmission as the creation of the enoki tops increases the reflection. However, additional increases in the height only slightly decrease the transmission. Fig. 4b plots the haze from 400 to 1200 nm as a function of nanostructure height for various structures. The optical haze factor is defined as the percent of scattered transmission to the total transmission:[22]

$$H(\lambda) = \left[\frac{\text{Scattered transmission}(\lambda)}{\text{Total transmission}(\lambda)} \right] \times 100\% \quad (5)$$

where λ is the free space wavelength. The portion of the total transmitted light that is considered scattered transmission is the
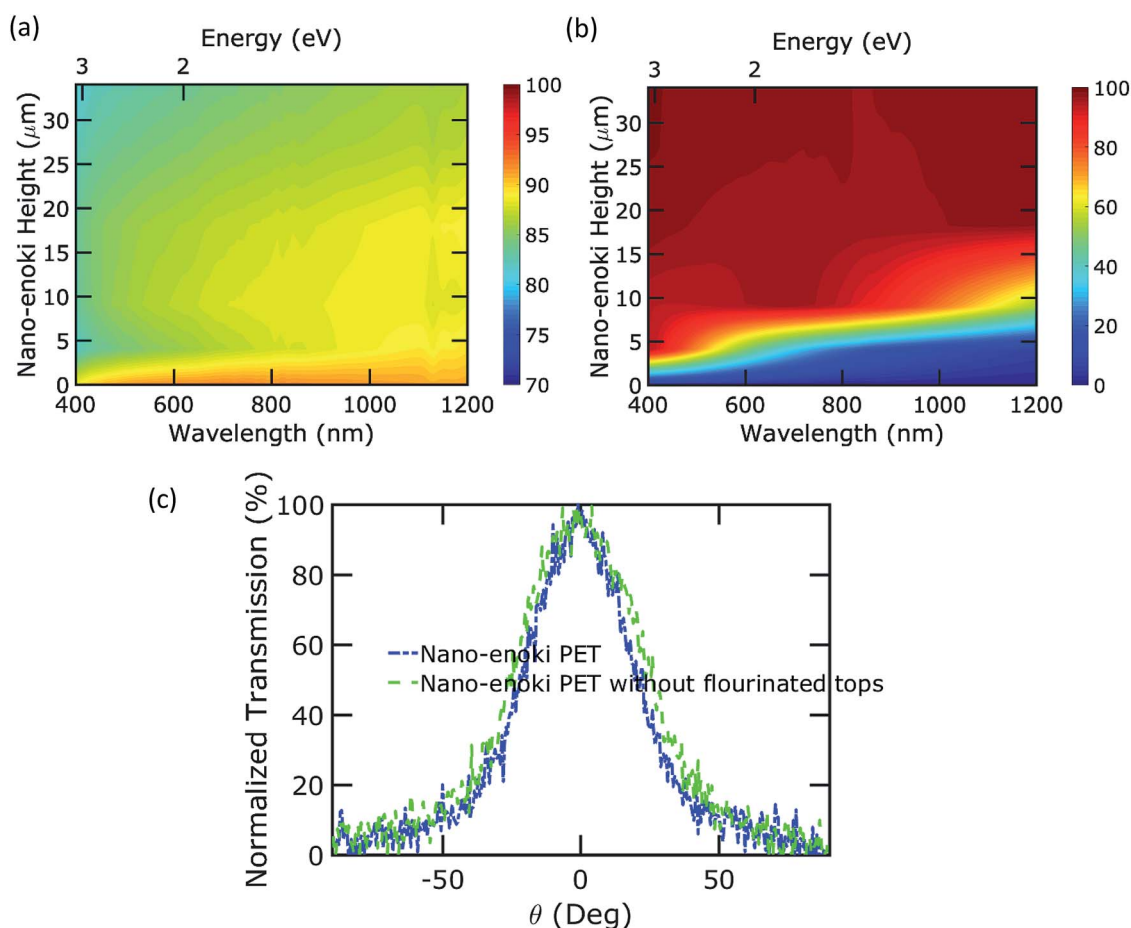

Fig. 4 Contour plots of (a) total transmission and (b) haze of nano-enoki PET as a function of wavelength and height. (c) shows the scattering angular distribution of transmission for nano-enoki with and without fluorinated tops.[25]
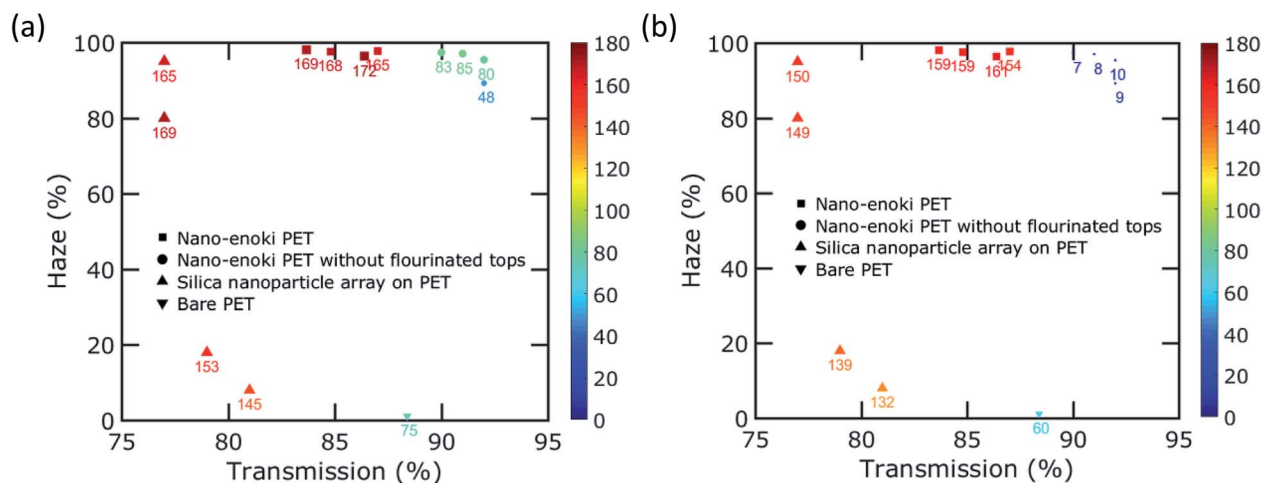
Fig. 5 Comparison of transparency (at a wavelength of 550 nm), haze (also at 550 nm) and (a) water and (b) ethylene glycol contact angle (in degrees) of our re-entrant nano-enoki PET, plain PET and silica nanoparticle array on PET,[24] the color and size of the data points correspond to the contact angle, which is also used to label each data point. The shape of each data point corresponds to the type of surface.

transmitted light that deviates from the incident beam greater than 2.5°. The total transmission was measured using an integrating sphere, which captures both the specular transmission and the scattered transmission, while the direct (or specular) transmission was measured without the integrating sphere. The scattered transmission is simply the difference between the total transmission and the direct transmission. The optical haze increases monotonically with the height of the nano-enoki PET.

We next characterized the angular distribution of the transmission through various substrates. Fig. 4c shows the scattering angular distribution of transmission for nano-enoki with and without fluorinated tops.[25] The scattering angle

range of both samples is more than 170° which shows strong light scattering capabilities and is much more than the scattering angles of ultrahigh haze nanostructured paper.[35] This figure also shows that the fluorination of the nano-enoki does not affect the scattering angle since it only forms a monolayer.[28,36–39]

Fig. 5 plots the wetting and photon management properties of the nano-enoki PET. In particular, Fig. 5a compares the water contact angle, transmission and haze, and Fig. 5b plots the ethylene glycol contact angle, transmission and haze of our nano-enoki PET in comparison with the data reported in Jeong *et al.*[24] As can be seen from these figures, the water contact
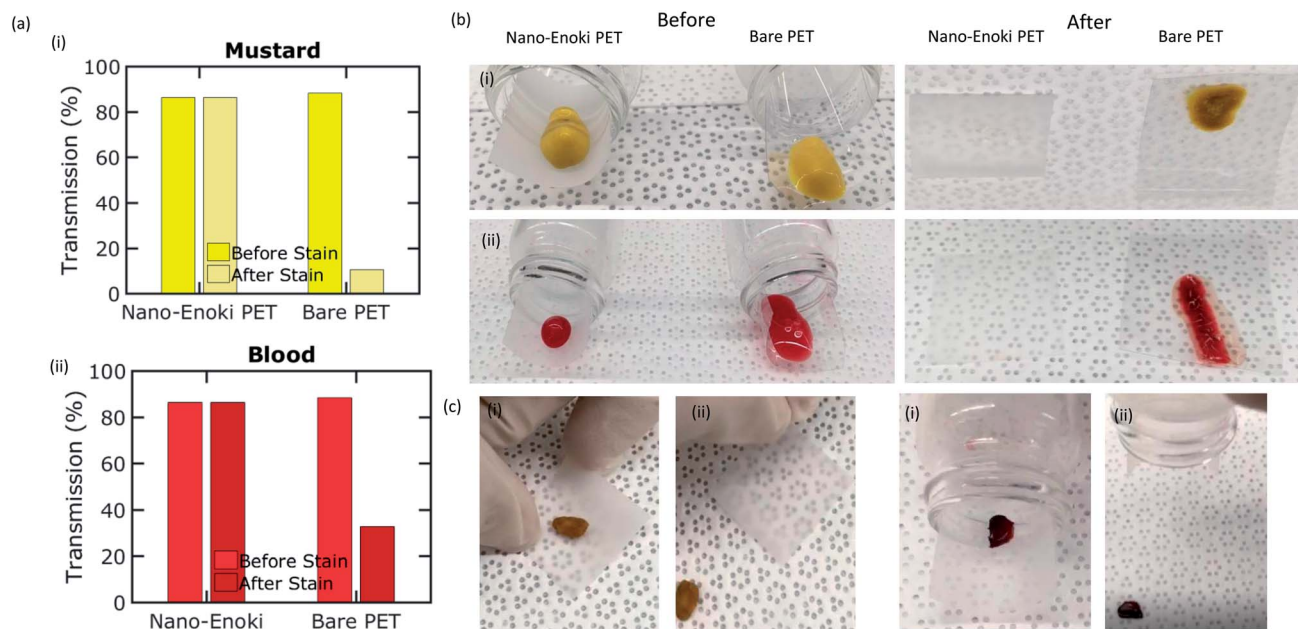

Fig. 6 (a) Transparency at 550 nm for nano-enoki PET and bare PET before and after staining of (i) mustard, and (ii) blood. (b) Optical images of (i) mustard, and (ii) blood stain before and after evaporation. (c) Optical pictures of dried mustard and blood droplets on nano-enoki (i) after drying and (ii) after tilting the substrate where the droplet simply flakes off the surface.
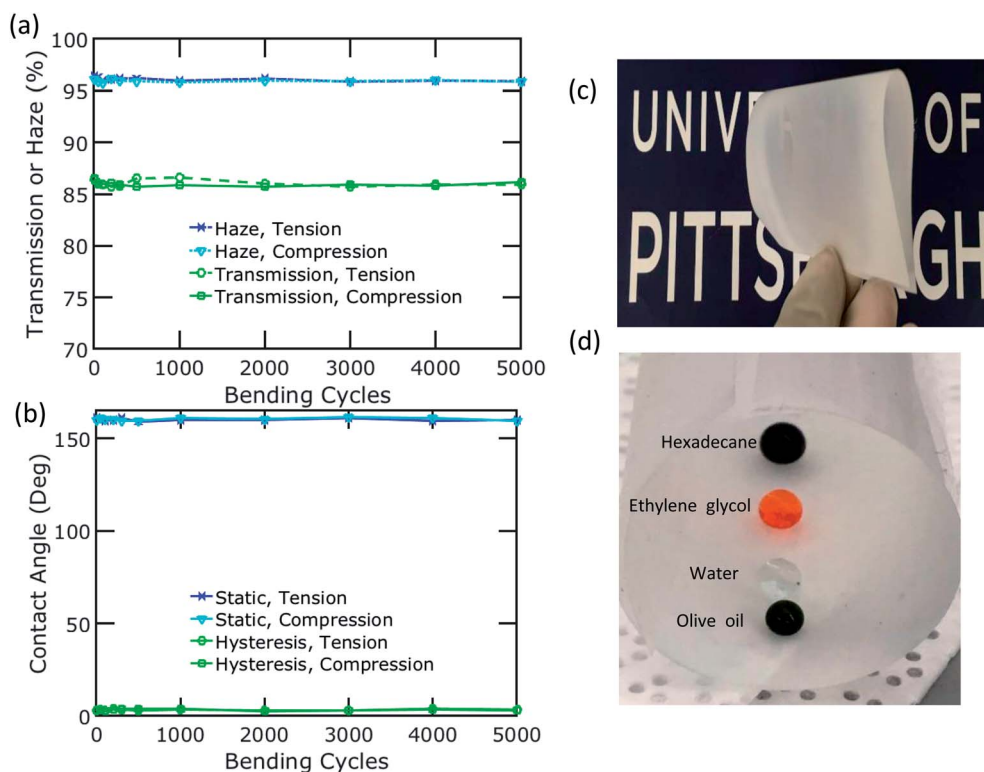
Fig. 7   (a) Transparency and haze at 550 nm and (b) oil contact angle and hysteresis as a function of bending cycles, for tension and compression. (c) Optical image of the flexibility of the substrate. (d) Optical image of different liquid droplets on curved PET. Food colors were added to the liquids in order to enhance visibility.

angle, oil contact angle, transparency and haze for our 18 μm height nano-enoki structure are 172 ± 1.5°, 161 ± 1.6°, 86.4%, and 96.4%, respectively, while the corresponding values for the best sample in their work are 165°, 150°, 77%, and 95%. Therefore, our work not only improves optical properties significantly, but also shows higher water and ethylene glycol contact angles. The hexadecane contact angle for our nano-enoki structures is 153 ± 1.7°, which is higher than 126° reported in the previous work of Jeong *et al.*

Next, we characterized the stain-resistance ability of our nano-enoki structures. Fig. 6a shows the stain test results for (i) mustard, and (ii) blood. The transparency at 550 nm for nano-enoki samples does not change after the stain test. In contrast, the transparency of bare PET reduces significantly after the stain test for mustard and blood. Fig. 6b shows the optical images of the (i) mustard, and (ii) blood. The mustard and blood tend to dry into small spots and easily flake off the nano-enoki PET surface after the sample is tilted due to the low infiltration of the liquid and repellency even after drying. In contrast, the mustard and blood spread over the bare PET and stay adhered to the surface. Fig. 6c shows dried mustard and blood droplets on nano-enoki (i) after drying and (ii) after tilting the sample where the dried drop simply flakes off the surface. Videos of the dried droplets flaking off the surface are attached in the ESI† as well as comparisons with the same stains on bare PET.

Fig. 7 plots the (a) transmission and haze at 550 nm wavelength and (b) ethylene glycol contact angle and hysteresis as a function of bending cycles of the 18 μm nano-enoki PET,

under tension and compression. Bending tests were conducted by bending the PET substrate around a stainless steel rod with a 1 inch diameter. Two samples with identical size, 3 cm × 3 cm, were placed under bending compression and tension by bending the etched surface towards and away from the steel rod, respectively. Fig. 7c and d show the optical images of flexibility of nano-enoki PET and different liquid droplets on a curved substrate. Neither the transmission nor haze nor oil contact angle nor hysteresis is changed significantly after 5000 cycles of bending, for either tension or compression. This suggests that the re-entrant enoki mushroom-like nano-structured PET is robust under bending and may be useful for flexible optoelectronic applications.

Conclusion

In conclusion, we demonstrate stain-resistant superomniphobic flexible optical PET based on nano-enoki structures. The nano-enoki structures demonstrate apparent contact angles over 150° and low contact angle hysteresis for a wide range of fluids with different surface tensions. This is in contrast to lotus leaf surfaces, which demonstrate low apparent contact angles and high contact angle hysteresis for olive oil and hexadecane. The fluorination and re-entrant tops of the nano-enoki provide stable Cassie–Baxter state wetting, where the low contact angle fraction between the droplets and PET enables high apparent contact angles and low contact angle hysteresis. The Cassie–Baxter state wetting is highly stable as breakthrough is not observed at pressures over 900 Pa,

which corresponds to a robustness factor over 17. In particular, the close spacing between nanostructures, which is the smallest of all re-entrant structures in the literature that we are aware of, provides high thermodynamic stability for the wetting. The nano-enoki structures demonstrate stain-resistance, where dried mustard and blood flake off the surface after tilting and the original transmission is recovered. The nano-enoki PET substrates are robust to bending and show similar transmission, haze, oil contact angle and hysteresis values after 5000 cycles of bending. These characteristics make the re-entrant nano-enoki PET a candidate for use in optoelectronic applications such as solar cells and LEDs where the combination of flexibility, high transmission, high haze, and stain-resistance is an important requirement.

Conflicts of interest

There are no conflicts to declare.

Acknowledgements

References

1 F. Ç. Cebeci, Z. Wu, L. Zhai, R. E. Cohen and M. F. Rubner, *Langmuir*, 2006, **22**, 2856–2862.

2 L. Cao, J. S. White, J. Park, J. A. Schuller, B. M. Clemens and M. L. Brongersma, *Nat. Mater.*, 2009, **8**, 643–647.

3 R. Fürstner, W. Barthlott, C. Neinhuis and P. Walzel, *Langmuir*, 2005, **21**, 956–961.

4 S. Haghanifar, P. Lu, M. Imrul Kayes, S. Tan, K.-J. Kim, T. Gao, P. Ohodnicki and P. W. Leu, *J. Mater. Chem. C*, 2018, **6**, 9191–9199.

5 T. Wu and Y. Suzuki, *Sens. Actuators, B*, 2011, **156**, 401–409.

6 S. Min Kang, S. Moon Kim, H. Nam Kim, M. Kyu Kwak, D. Ha Tahk and K. Y. Suh, *Soft Matter*, 2012, **8**, 8563–8568.

7 J. Choi, W. Jo, S. Y. Lee, Y. S. Jung, S.-H. Kim and H.-T. Kim, *ACS Nano*, 2017, **11**, 7821–7828.

8 X. Liu, H. Gu, M. Wang, X. Du, B. Gao, A. Elbaz, L. Sun, J. Liao, P. Xiao and Z. Gu, *Adv. Mater.*, 2018, **30**, 1800103.

9 P. Zhu, T. Kong, X. Tang and L. Wang, *Nat. Commun.*, 2017, **8**, 15823.

10 G.-T. Yun, W.-B. Jung, M. S. Oh, G. M. Jang, J. Baek, N. I. Kim, S. G. Im and H.-T. Jung, *Sci. Adv.*, 2018, **4**, eaat4978.

11 L. Brown, J. M. Wolf, R. Prados-Rosales and A. Casadevall, *Nat. Rev. Microbiol.*, 2015, **13**, 620.

12 S. Pan, A. K. Kota, J. M. Mabry and A. Tuteja, *J. Am. Chem. Soc.*, 2013, **135**, 578–581.

13 W. Choi, A. Tuteja, S. Chhatre, J. M. Mabry, R. E. Cohen and G. H. McKinley, *Adv. Mater.*, 2009, **21**, 2190–2195.

14 B. Leng, Z. Shao, G. de With and W. Ming, *Langmuir*, 2009, **25**, 2456–2460.

15 Y. Yao, J. Tao, J. Zou, B. Zhang, T. Li, J. Dai, M. Zhu, S. Wang, K. Kelvin Â Fu, D. Henderson, E. Hitz, J. Peng and L. Hu, *Energy Environ. Sci.*, 2016, **9**, 2278–2285.

16 G. Tan, J.-H. Lee, Y.-H. Lan, M.-K. Wei, L.-H. Peng, I.-C. Cheng and S.-T. Wu, *Optica*, 2017, **4**, 678–683.

17 M. Wen, J. Zhong, S. Zhao, T. Bu, L. Guo, Z. Ku, Y. Peng, F. Huang, Y.-B. Cheng and Q. Zhang, *J. Mater. Chem. A*, 2017, **5**, 8352–8359.

18 F. Li, M. Du and Q. Zheng, *ACS Nano*, 2016, **10**, 2910–2921.

19 M. Deng, R. James, C. T. Laurencin and S. G. Kumbar, *IEEE Transactions on NanoBioscience*, 2012, **11**, 3–14.

20 L. Müller-Meskamp, Y. H. Kim, T. Roch, S. Hofmann, R. Scholz, S. Eckardt, K. Leo and A. F. Lasagni, *Adv. Mater.*, 2012, **24**, 906–910.

21 T.-H. Han, Y. Lee, M.-R. Choi, S.-H. Woo, S.-H. Bae, B. H. Hong, J.-H. Ahn and T.-W. Lee, *Nat. Photonics*, 2012, **6**, 105–110.

22 T. Gao, S. Haghanifar, M. G. Lindsay, P. Lu, M. I. Kayes, B. D. Pafchek, Z. Zhou, P. R. Ohodnicki and P. W. Leu, *Adv. Opt. Mater.*, 2018, **6**(9), 1700829.

23 C. Preston, Y. Xu, X. Han, J. N. Munday and L. Hu, *Nano Res.*, 2013, **6**, 461–468.

24 E. Jeong, G. Zhao, M. Song, S. Min Yu, J. Rha, J. Shin, Y.-R. Cho and J. Yun, *J. Mater. Chem. A*, 2018, **6**, 2379–2387.

25 S. Haghanifar, R. T. R. D. Vecchis, K.-J. Kim, J. Wuenschell, S. P. Sharma, P. Lu, P. Ohodnicki and P. W. Leu, *Nanotechnology*, 2018, **29**, 42LT01.

26 K. Nojiri, *Dry Etching Technology for Semiconductors*, Springer, 2012.

27 S. Haghanifar, T. Gao, R. T. R. D. Vecchis, B. Pafchek, T. D. B. Jacobs and P. W. Leu, *Optica*, 2017, **4**, 1522–1525.

28 D. Nanda, P. Varshney, M. Satapathy, S. S. Mohapatra and A. Kumar, *Colloids Surf., A*, 2017, **529**, 231–238.

29 W. Barthlott and C. Neinhuis, *Planta*, 1997, **202**, 1–8.

30 J. Drelich and E. Chibowski, *Langmuir*, 2010, **26**, 18621–18623.

31 Y. C. Jung and B. Bhushan, *Scr. Mater.*, 2007, **57**, 1057–1060.

32 A. Tuteja, W. Choi, J. M. Mabry, G. H. McKinley and R. E. Cohen, *Proc. Natl. Acad. Sci. U. S. A.*, 2008, **105**, 18200–18205.

33 K. Golovin, D. H. Lee, J. M. Mabry and A. Tuteja, *Angew. Chem., Int. Ed.*, 2013, **52**, 13007–13011.

34 A. K. Kota, Y. Li, J. M. Mabry and A. Tuteja, *Adv. Mater.*, 2012, **24**, 5838–5843.

35 Z. Fang, H. Zhu, Y. Yuan, D. Ha, S. Zhu, C. Preston, Q. Chen, Y. Li, X. Han, S. Lee, G. Chen, T. Li, J. Munday, J. Huang and L. Hu, *Nano Lett.*, 2014, **14**, 765–773.

36 R. H. Tredgold, *Order in Thin Organic Films*, Cambridge University Press, 1994.

37 S. A. Mahadik, M. S. Kavale, S. K. Mukherjee and A. V. Rao, *Appl. Surf. Sci.*, 2010, **257**, 333–339.

38 J. X. H. Wong and H.-Z. Yu, *J. Chem. Educ.*, 2013, **90**, 1203–1206.

39 S. Haghanifar, M. McCourt, B. Cheng, J. Wuenschell, P. Ohodnicki and P. W. Leu, *Mater. Horiz.*, 2019, accepted manuscript.